GSA Data Repository Item 2017076
Goudge, T.A., Russell, J.M., Mustard, J.F., Head, J.W., and Bijaksana, S., 2017, A 40,000 yr record of clay mineralogy at Lake Towuti, Indonesia: Paleoclimate reconstruction from reflectance spectroscopy and perspectives on paleolakes on Mars: GSA Bulletin, doi:10.1130/B31569.1.

ADDITIONAL DETAIL ON METHODS

VNIR Spectroscopy Methods

All spectra collected with the ASD FieldSpec were measured relative to the reflectance of a Spectralon® panel and corrected for the absolute reflectance properties of Spectralon®. The external light source used to illuminate the input sediment samples and lake core subsamples is a 60 W quartz tungsten halogen lamp, and was oriented with an approximate incidence angle of 30°. Reflectance was measured with the bare ASD fiber optic cable, which has a field of view of 25° and was positioned with an approximate emission angle of 0° ~1–3 cm from the sample. For each sample, three sets of 100 reflectance measurements were collected, and all 300 measurements were averaged together to reduce noise. Additionally, for the >1 mm and 0.25–1 mm grain size separates, the reflectance spectra for each set of 100 measurements were collected from different spots on a prepared surfaced and averaged together to ensure that the spectrum of the sample is not overly influenced by the spectral properties of a small number of large, individual grains.

The contact probe used to measure the two lake cores illuminates a contacted sample at an incidence angle of ~0° and measures the reflected light from a spot ~1 cm^2 in size (~0.9 × 1.2 cm) at an emission angle of ~35°. The freeze-dried core U-channels were fed through the Geotek™ MSCL at 1 cm step intervals, and at each step the sensor stage was lowered so that the contact probe came into contact with the core surface, and 50 reflectance measurements were made using the ASD FieldSpec. The measurements for each step were averaged together, which resulted in a data set that contains a single spectrum for each ~1 cm of core surface along the entire ~10 m length of each of the two cores.

Age Model Development

To convert our data set of scanned VNIR reflectance data for the two sediment cores from core depth to age, we developed two simple linear interpolated age models (Fig. DR3). Magnetic susceptibility data from core TOW4 were compared to magnetic susceptibility data from the Lake Towuti sediment core Co1230, which was collected from approximately the same location as core TOW4 and dated using 12 bulk organic carbon ^{14}C dates and a smooth-spline fit function (Vogel et al., 2015). We chose 13 tie-points where specific peaks, or series of peaks, could confidently be identified in both magnetic susceptibility data sets, and extracted ages from core Co1230 at these points. A linear interpolated age model was then created for the entire TOW4 core length using these 13 tie-points (Fig. DR3A) and the Arand software package (Howell et al., 2006).

The age model for core TOW5 was created using the same method, with the exceptions that only 10 tie-points were used (Fig. DR3B), and that the magnetic susceptibility data from core TOW5 were instead compared to magnetic susceptibility data from sediment core TOW9

collected ~1.8 km southeast from TOW5 (Russell et al., 2014), which is justified by the excellent agreement in the magnetic susceptibility data of TOW9 and Co1230 (Vogel et al., 2015). The original TOW9 age model is based on 20 bulk organic carbon ^{14}C dates and three terrestrial macrofossil ^{14}C dates, which were interpolated using a mixed-effect regression model (Russell et al., 2014).

Major Element Chemistry Methods (ICP-AES)

Elemental concentrations (Al, Ca, Cr, Fe, K, Mg, Mn, Na, Ni, Si, and Ti) were determined from ICP-AES runs using the intensities of peaks at the wavelengths detailed by Murray et al. (2000), and linear regressions from 10 standard reference materials (NIST standards 1c, 1646, 2711, and 2702, and USGS standards G-2, BCR-2, DTS-2B, SGR-1, BHVO-2, and MAG-1). We also corrected for instrument background and drift using blank and drift measurements. Six samples were run in triplicate to assess reproducibility, and these measurements have low inter-replicate elemental variability (~5% variation on average), suggesting high precision for our elemental abundance results.

VNIR Spectroscopy Analysis

We developed a parameter, BD1975:BD1915, to quantify changes in the shape of the ~1900 nm absorption feature in our VNIR reflectance data (Fig. 3). This parameter is calculated as:

$$\text{BD1975:BD1915} = BD_{1975}/BD_{1915} \quad \text{(DR1)}$$

where BD_C is the band depth at wavelength λ_C (Fig. 3A). Band depth is calculated from the equations:

$$BD_C = 1 - \frac{R_C}{(1-a) \times R_S + a \times R_L} \quad \text{(DR2)}$$

$$a = \frac{\lambda_C - \lambda_S}{\lambda_L - \lambda_S} \quad \text{(DR3)},$$

where R_C is the measured reflectance at λ_C, R_S is the measured reflectance at the short wavelength continuum tie point located at wavelength λ_S, and R_L is the measured reflectance at the long wavelength continuum tie point located at wavelength λ_L (Clark and Roush, 1984; Clark, 1999; Pelkey et al., 2007). For the BD1975:BD1915 parameter, the short wavelength continuum tie point is an average of points from 1820 to 1850 nm and the long wavelength continuum tie point is an average of points from 2065 to 2075 nm. The band center for BD_{1975} is an average of points from 1965 to 1980 nm, and the band center for BD_{1915} is an average of points from 1905 to 1920 nm.

Additionally, we compared the BD1975:BD1915 parameter to the BD2200 parameter (Fig. DR2), which measures the band depth of the Al-OH absorption centered near ~2200 nm. This parameter used the formulation given in Equations DR2 and DR3, with a short wavelength continuum tie point taken as an average of points from 2155 to 2165 nm, a long wavelength continuum tie point taken as an average of points from 2225 to 2235 nm, and the band center

taken as an average of points from 2200 to 2215 nm. The BD1975:BD1915 parameter and the BD2200 parameter have a strong negative correlation, indicating stronger ~2200 nm absorptions are associated with narrower ~1900 nm absorptions.

REFERENCES CITED

Clark, R.N., 1999, Spectroscopy of rocks and minerals, and principles of spectroscopy, *in* Rencz, A.N., ed., Remote Sensing for the Earth Sciences: Manual of Remote Sensing, 3rd ed., v. 3.: New York, John Wiley & Sons, Inc., p. 3–58.

Clark, R.N., and Roush, T.L., 1984, Reflectance spectroscopy: Quantitative analysis techniques for remote sensing applications: Journal of Geophysical Research, v. 89, p. 6329–6340, doi:10.1029/JB089iB07p06329.

Howell, P., Pisias, N., Ballance, J., Baughman, J., and Ochs, L., 2006, ARAND time-series analysis software: Brown University, Providence, RI, http://www.ncdc.noaa.gov/paleo/softlib/arand/download.html.

Murray, R.W., Miller, D.J., and Kryc, K.A., 2000, Analysis of major and trace elements in rocks, sediments, and interstitial waters by inductively coupled plasma–atomic emission spectrometry (ICP-AES): ODP Techical Note, v. 29, p. 1–27.

Pelkey, S.M., Mustard, J.F., Murchie, S., et al., 2007, CRISM multispectral summary products: Parameterizing mineral diversity on Mars from reflectance: Journal of Geophysical Research, v. 112, p. E08S14, doi:10.1029/2006JE002831.

Russell, J.M., Vogel, H., Konecky, B.L., Bijaksana, S., Huang, Y., Melles, M., Wattrus, N., Costa, K., and King, J.W., 2014, Glacial forcing of central Indonesian hydroclimate since 60,000 y B.P: Proceedings of the National Academy of Sciences of the United States of America, v. 111, p. 5100–5105, doi:10.1073/pnas.1402373111.

Vogel, H., Russell, J.M., Cahyarini, S.Y., Bijaksana, S., Wattrus, N., Rethemeyer, J., and Melles, M., 2015, Depositional modes and lake-level variability at Lake Towuti, Indonesia during the past ~29 kyr BP: Journal of Paleolimnology, v. 54, p. 359–377, doi:10.1007/s10933-015-9857-z.

TABLE DR1. MAJOR ELEMENT CHEMISTRY FOR INPUT SEDIMENT AND LAKE CORE SUBSAMPLES*

Sample	Details†	Al_2O_3	CaO	Cr_2O_3	FeO	K_2O	MgO	MnO	Na_2O	NiO	SiO_2	TiO_2
Input Sediment												
Bedload	>1 mm	2.01	1.34	0.37	9.15	0.00	33.43	0.19	0.04	0.40	41.65	0.04
	0.25-1 mm	4.00	1.26	1.62	9.90	0.10	25.40	0.15	0.14	0.35	39.37	0.14
	63-250 μm	**3.39**	**1.02**	**0.88**	**9.62**	**0.10**	**26.22**	**0.14**	**0.12**	**0.37**	**40.52**	**0.12**
	32-63 μm	5.42	1.80	1.02	9.90	0.24	19.81	0.17	0.28	0.36	42.36	0.24
	<32 μm	5.68	1.87	0.97	10.64	0.28	17.51	0.19	0.32	0.38	41.09	0.28
	Bulk	3.92	1.27	1.01	9.78	0.13	25.52	0.16	0.16	0.37	41.82	0.17
Suspended	0.25-1 mm	2.29	1.28	0.39	10.91	0.03	29.37	0.14	0.09	0.33	42.90	0.05
Load	**63-250 μm**	**3.16**	**0.75**	**0.35**	**10.24**	**0.13**	**26.81**	**0.16**	**0.11**	**0.34**	**41.96**	**0.10**
	32-63 μm	5.39	1.73	0.95	10.08	0.29	21.50	0.18	0.28	0.29	42.07	0.24
	<32 μm	5.87	1.24	0.50	10.32	0.48	15.70	0.17	0.42	0.31	40.98	0.24
	Bulk	4.37	1.25	0.50	10.42	0.25	21.13	0.19	0.17	0.32	41.68	0.17
River	>1 mm	1.49	0.69	0.36	10.65	0.01	30.31	0.17	0.02	0.34	39.82	0.02
Mouth	0.25-1 mm	2.51	0.99	0.56	10.35	0.03	30.06	0.11	0.07	0.31	41.57	0.05
Sediment	**63-250 μm**	**3.19**	**1.22**	**0.53**	**9.31**	**0.07**	**27.47**	**0.14**	**0.15**	**0.32**	**45.20**	**0.12**
	32-63 μm	4.55	1.47	0.84	7.20	0.17	16.27	0.25	0.27	0.28	38.53	0.19
	<32 μm	4.49	1.34	0.63	6.75	0.20	15.21	0.29	0.30	0.29	40.92	0.21
	Bulk	1.83	0.89	0.38	10.33	0.01	29.62	0.14	0.05	0.33	39.37	0.03
Core TOW4												
C4-1	2783	7.32	0.59	0.47	15.32	0.41	17.59	0.26	0.14	0.48	41.16	0.28
C4-2	4173	10.43	0.53	0.43	16.90	0.73	11.78	0.23	0.18	0.56	42.53	0.42
C4-3	**6025**	**6.59**	**0.60**	**0.41**	**15.53**	**0.41**	**17.60**	**0.33**	**0.14**	**0.41**	**40.18**	**0.24**
C4-4	8053	8.48	0.44	0.38	16.68	0.70	15.07	0.25	0.13	0.44	39.53	0.32
C4-5	9046	6.05	0.82	0.41	12.69	0.44	20.85	0.20	0.22	0.35	41.28	0.25
C4-6	10791	10.89	0.43	0.41	17.13	1.09	10.91	0.15	0.20	0.42	42.06	0.42
C4-7	11579	7.47	0.83	0.43	13.69	0.55	17.62	0.23	0.23	0.36	43.53	0.29
C4-8	13165	6.10	0.67	0.40	14.16	0.54	21.07	0.38	0.18	0.37	41.93	0.24
C4-9	**14862**	**3.97**	**0.60**	**0.41**	**13.90**	**0.29**	**24.64**	**0.26**	**0.06**	**0.40**	**37.78**	**0.14**
C4-10	15483	7.00	0.50	0.66	18.97	0.94	18.53	0.12	0.06	0.63	37.61	0.22
C4-11	19532	1.59	0.39	0.30	9.23	0.02	34.54	0.14	0.01	0.32	41.60	0.03
Core TOW5												
C5-1	1725	10.37	0.56	0.45	18.40	0.58	10.27	0.14	0.17	0.51	41.18	0.42
C5-2	5662	6.16	0.53	0.40	14.84	0.36	20.76	0.21	0.11	0.41	40.76	0.22
C5-3	11083	11.25	0.43	0.31	14.33	1.40	12.04	0.11	0.31	0.33	47.74	0.47
C5-4	**16989**	**2.81**	**0.47**	**0.41**	**12.99**	**0.16**	**27.89**	**0.45**	**0.04**	**0.35**	**36.92**	**0.09**
C5-5	22548	7.98	0.42	0.60	23.77	0.37	14.61	0.35	0.04	0.61	35.47	0.29
C5-6	26015	3.01	0.51	0.52	13.80	0.08	28.94	0.55	0.02	0.38	38.57	0.09
C5-7	27041	3.27	0.38	0.43	13.26	0.10	27.77	0.11	0.02	0.41	39.14	0.09
C5-8	32010	6.82	0.57	0.42	15.36	0.40	18.33	0.22	0.10	0.37	39.48	0.23
C5-9	36989	7.53	0.47	0.55	22.58	0.40	13.35	1.46	0.08	0.55	36.18	0.28
C5-10	38631	11.92	0.46	0.32	15.60	1.24	10.55	0.21	0.20	0.42	45.61	0.47

*All listed values are reported in wt%. Rows listed in bold are the samples that were run in triplicate. Value listed is the mean concentration for all three runs.

†For input sediment, column lists the grain size of the sample, and for lake core subsamples, column lists the age (in yr BP) of the sample from the interpolated age model.

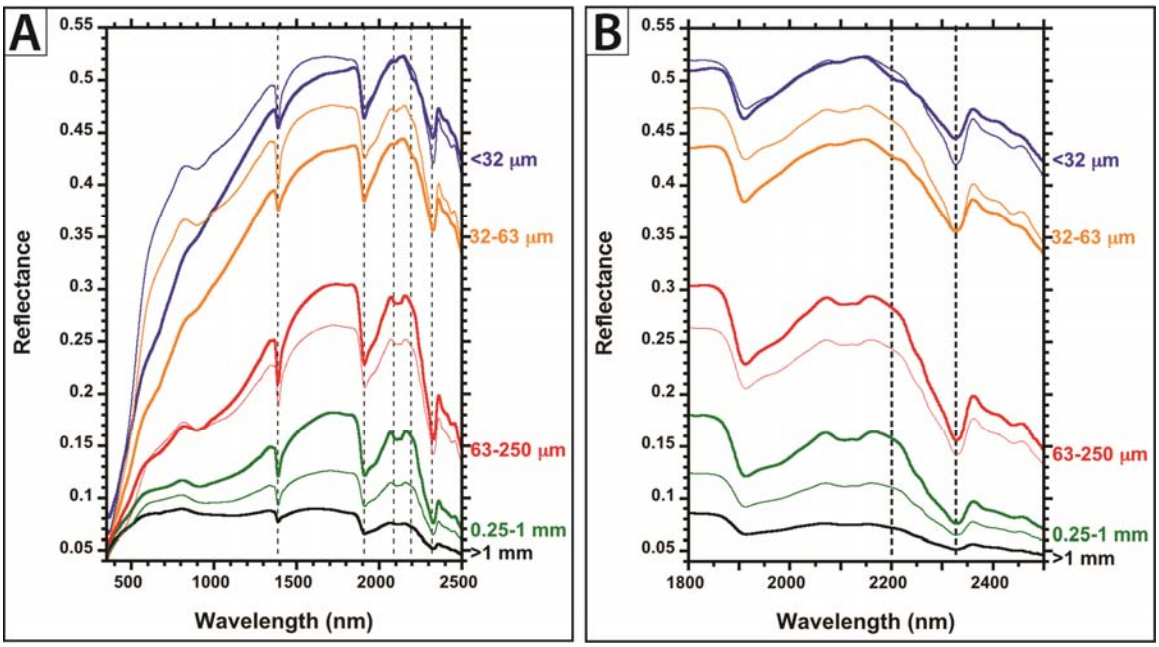

Figure DR1. VNIR reflectance spectra of natural and powdered grain size separates for the Mahalona River mouth sediment. Natural grain size separates are thick lines, and powdered grain size separates are thin lines. (A) Full VNIR reflectance spectra. Dashed lines are located at ~1400, 1900, 2100, 2200, and 2320 nm. (B) Spectral signature from 1800 to 2500 nm, highlighting the prominent change in the ~1900 nm absorption shape and the ~2200 nm absorption. Dashed lines are located at ~2200 and 2320 nm.

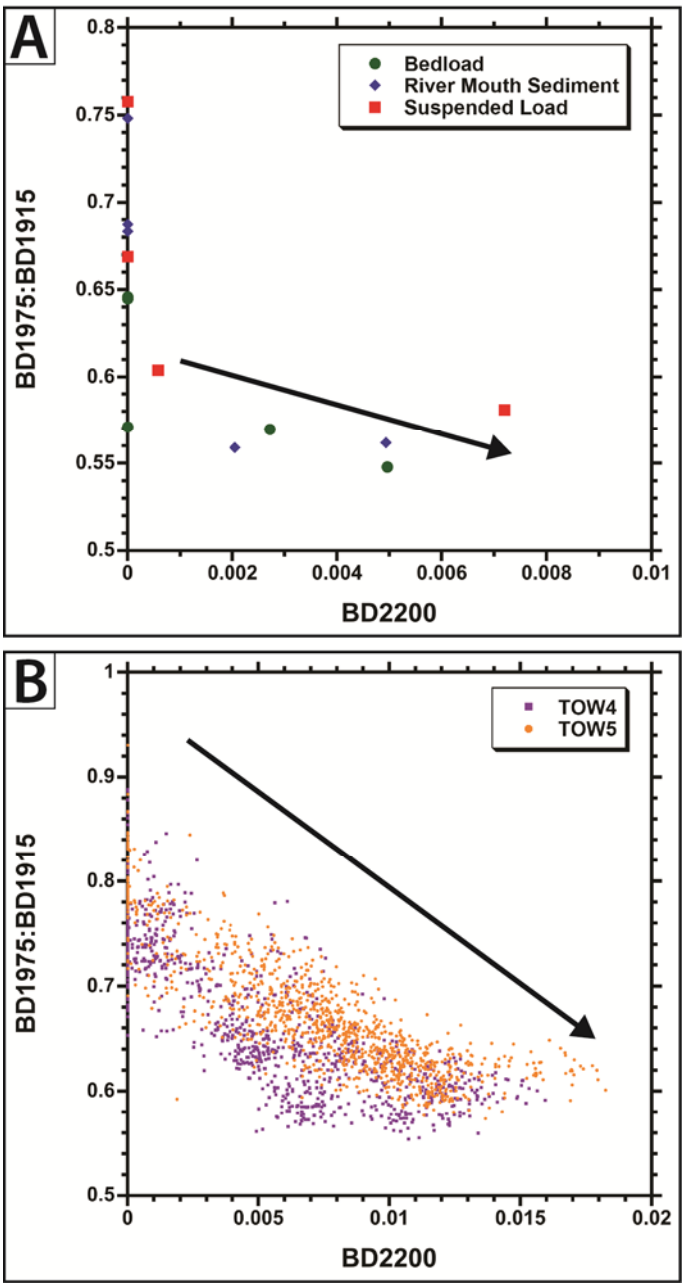

Figure DR2. BD1975:BD1915 versus BD2200 for input river sediment from the Mahalona River (A) and lake core sediment (B). Note the strong negative correlation.

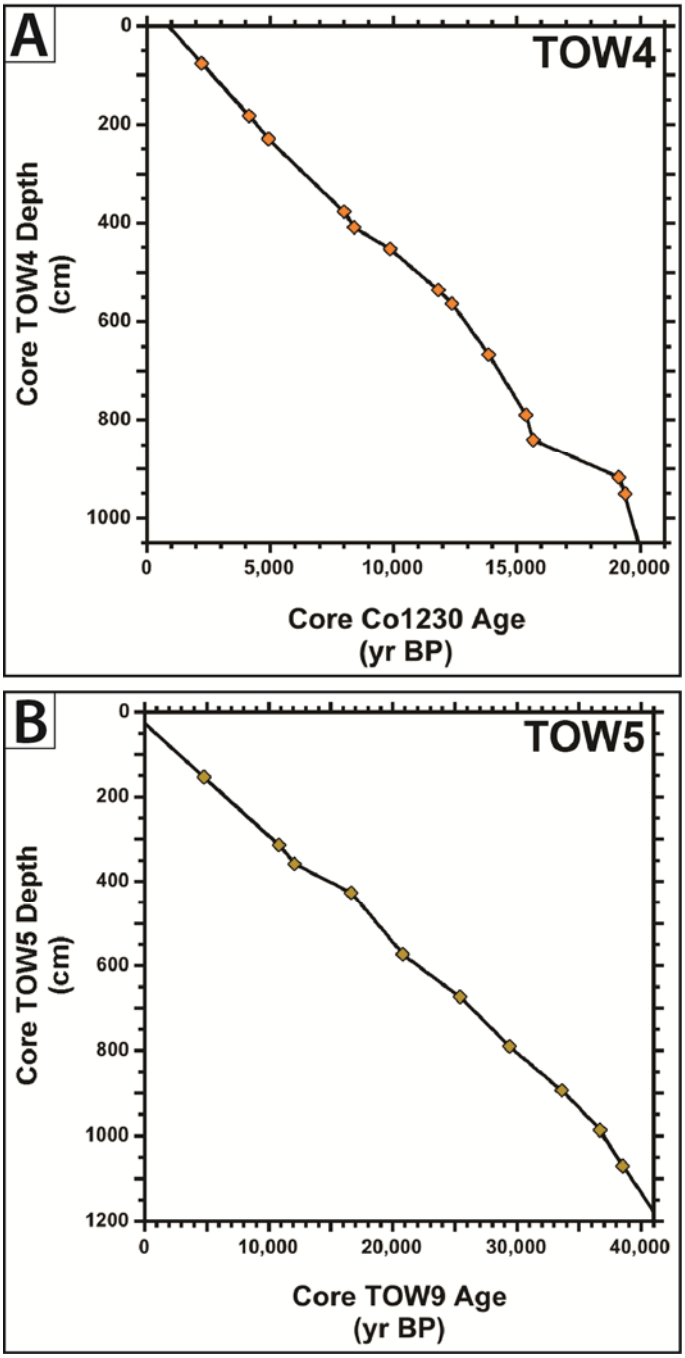

Figure DR3. Depth-age plot for tie-points from cores TOW4 (A) and TOW5 (B) used for calculating linear interpolated age models (shown in black lines).